Nat. Hazards Earth Syst. Sci. Discuss., doi:10.5194/nhess-2016-193, 2016
Manuscript under review for journal Nat. Hazards Earth Syst. Sci.
Published: 3 June 2016

Natural Hazards and Earth System Sciences
Discussions

Analysing post-earthquake landslide activity using multi-temporal landslide inventories near the epicentral area of the 2008 Wenchuan earthquake

Chenxiao Tang [1,2], Cees J. Van Westen [1], Hakan Tanyaş [1], Victor G. Jetten [1],

[1]Faculty of Geo-Information Sciences and Earth Observation (ITC), University of Twente, the Netherlands
[2]State Key Laboratory for Geohazard Prevention and Environmental Protection (SKLGP), Chengdu University of Technology

Correspondence to: Chenxiao Tang (c.tang@utwente.nl)

Abstract. Large earthquakes in mountainous regions may trigger thousands of landslides, some active for years. We analysed the changes in landslide activity near 2008 Wenchuan earthquake epicentre, generating five landslide inventories for different years through stereoscopic digital visual image interpretation. From May 2008 to April 2015, 660 new landslides occurred outside the co-seismic landslide areas. In April 2015, the number of active landslides had gone down to 66, less than 1% of the co-seismic landslides, still much higher than the pre-earthquake situation. We expect that the landslide activity will continue to decay, but may be halted if extreme rainfall events occur.

Keywords: multi-temporal; landslide inventories; post-earthquake landslides; Wenchuan earthquake; image interpretation;

Introduction

Large earthquakes can cause huge losses to human society due to ground shaking, fault rupture, liquefaction, tsunamis and also due to co-seismic landslides that can be triggered in mountainous areas. Some examples of earthquake-triggered landslide events are the 1976 Guatemala earthquake, with 50,000 landslides (Harp et al., 1981), the 1994 Northridge Earthquake in California with more than 11,000 landslides (Harp and Jibson, 1995), the 1999 Chi-Chi earthquake in Taiwan with 26,000 co-seismic landslides (Cheng et al., 2005), and the 2008 Wenchuan earthquake in China with more than 56,000 landslides (Dai et al., 2011b). In areas that have been affected by such large earthquakes, the threat of landslides persists in the years following the earthquake, as huge amounts of deposits loosened by the earthquake on hillslopes provide sufficient source materials for landslide reactivations and debris flow occurrences during heavy rainstorms.

After the 1999 Chi-Chi earthquake (Mw 7.6), a number of extreme precipitation events reactivated the co-seismic landslides and triggered several catastrophic mass movements. Two examples are: the debris flow which destroyed Daxing village on 30 July 2001, and the landslide that buried Hsiaolin village forming a barrier lake in 2009 (Dong et al., 2011). Many studies about post-earthquake landslides were carried out after the Chi-Chi earthquake, including Fan et al. (2003), Chang et al. (2006), Lin et al. (2006).

Nat. Hazards Earth Syst. Sci. Discuss., doi:10.5194/nhess-2016-193, 2016
Manuscript under review for journal Nat. Hazards Earth Syst. Sci.
Published: 3 June 2016

Natural Hazards and Earth System Sciences
Discussions

Also the devastating Wenchuan earthquake (M_w 7.9) which occurred in the western part of Sichuan province in China on May 12, 2008, demonstrated the post-seismic landslide problem. In the years following the earthquake, several catastrophic debris flows occurred. Some example are the debris flows that destroyed part of Beichuan town on September 24 2008, the debris flow which dammed the Minjiang River on August 13 2010, and the debris flow which damaged Qipangou village on July 10 2013(Tang et al., 2009; Xu et al., 2012). These post-earthquake mass movements highlighted the need for more research to provide critical information for assessing post-earthquake landslide hazards as a basis for reconstruction planning in earthquake affected mountain areas. The majority of the research thus far in the Wenchuan area focused on the analysis of case studies on post-seismic landslide mechanisms. Limited research has concentrated on the long-term evolution of landslide activities, and the changes in the geo-environment after earthquakes. For the Chi-Chi earthquake area, Hovius et al. (2011) analysed the long-term erosion and mass balance effects of the earthquake. They concluded that the enhanced mass wasting and sediment removal after the earthquake was more than five times the pre-earthquake rate, and it required about six years to return to pre-earthquake levels. The analysis of changes in landslide activity is based on the analysis of satellite images over a number of years. For the Chi-Chi earthquake this was reported by several authors (Lin et al., 2008; Shieh, 2009; Shou et al., 2011a; Shou et al., 2011b). For the Wenchuan earthquake area, some researchers have studied the short term (within 3 years) changes in landslide reactivation after storms(Tang et al., 2011; Zhou and Tang, 2014). Huang and Fan (2013) made a prediction that it will take about 20 years before the landslide activity will return to pre-earthquake levels; however, this was not based on long-term studies.

The objective of this research is to contribute to the long term monitoring of post-earthquake landslide activity in the Wenchuan area through the use of multi-temporal remote sensing images. A series of landslide inventories for the period up to 2015 were generated, and several controlling factors were analysed.

Study Area

The study area (Fig. 1) is located near the epicentre of the Wenchuan earthquake, around Yingxiu Town and Longchi Town, in Sichuan province, China. The study area covers approximately 179 Km^2. The elevation of the study area varies from 767 m to 3950 m, with an average of 1736m. The Yingxiu area, the western side of the study area, is steeper than the Longchi area (eastern side). Areas with slopes steeper than 45 ℃overs 21% of Yingxiu and only 2% of the Longchi area. The major fault rupture of the Wenchuan earthquake (Yingxiu- Beichuan fault) passes through the area. The predominant lithology in the area is granite (59% of the area), diorite (covers 22% of the area) in the western part, and some sedimentary rocks in the south-eastern part which are bounded by faults. The climate in the study area is humid subtropical with an annual average temperature of 13℃. The average yearly precipitation in the area is 1134 mm, and 70% of the precipitation occurs from June to September. The highest precipitation is in August, with an average monthly rainfall of 289.9 mm. The recorded maximum monthly, daily, and hourly precipitation amounts are 593 mm , 234 mm and 84 mm respectively (Luo et al., 2010)

Nat. Hazards Earth Syst. Sci. Discuss., doi:10.5194/nhess-2016-193, 2016
Manuscript under review for journal Nat. Hazards Earth Syst. Sci.
Published: 3 June 2016

Natural Hazards and Earth System Sciences
Discussions

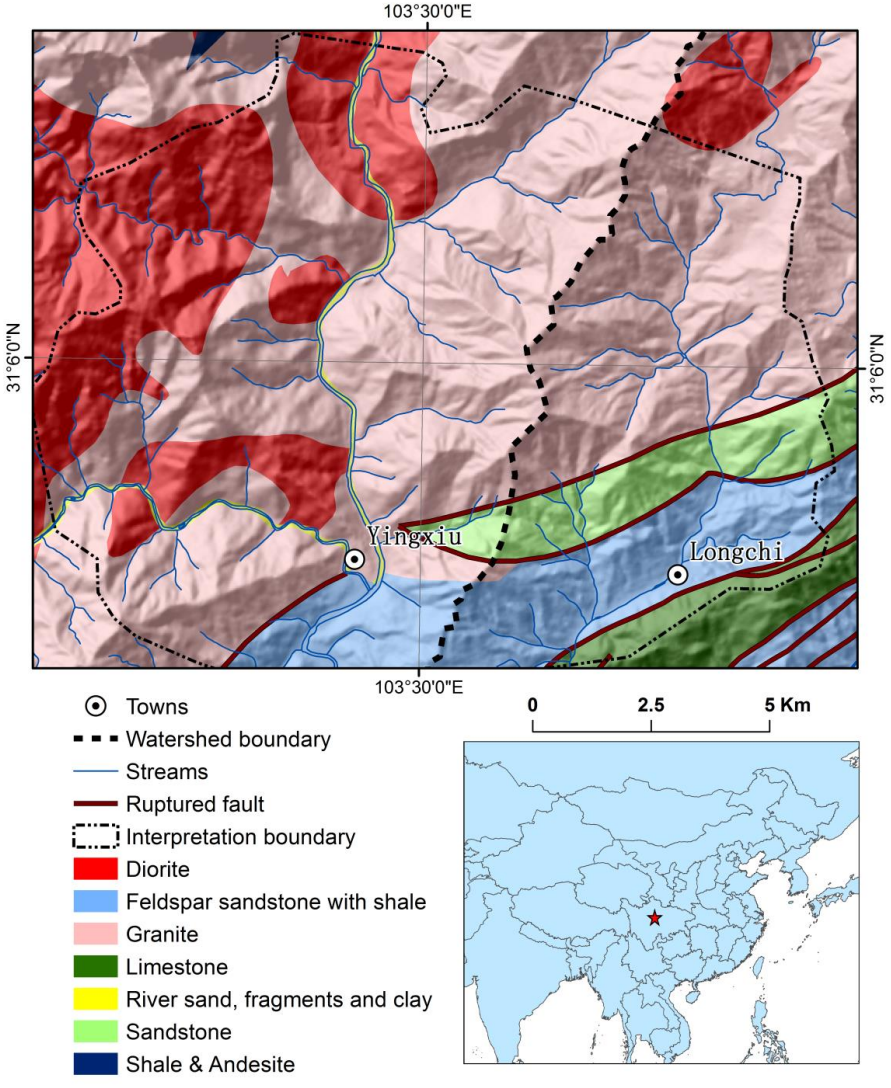

Figure 1 Map of the study area. The west part of the thick dotted line is the Yingxiu area and the east part is the Longchi area. The area for which the landslide interpretation was carried out is shown as a polygon with a thin dotted border.

Data & Methods

Remote sensing images and other data

We have acquired multiple remote sensing images from various sources for making multi-temporal landslide inventories. Based on the resolution, cloud coverage, and shadows, a total of 6 images taken in

Nat. Hazards Earth Syst. Sci. Discuss., doi:10.5194/nhess-2016-193, 2016
Manuscript under review for journal Nat. Hazards Earth Syst. Sci.
Published: 3 June 2016

Natural Hazards and Earth System Sciences Discussions

2008, 2009, 2011, 2013 and 2015 were selected to monitor the landslide activities after the earthquake and 1 image was selected from 2005 representing the pre-earthquake situation (Table 1). All images were geometrically corrected with Erdas Autosync Workstation, using a GCP-referenced image. To assist landslide digitizing with stereo visualization and to analyse controlling factors of post-seismic landslide activities, a Digital Elevation Model derived from 20m-interval contour lines was collected from the State Key Laboratory of Geo-hazard Prevention and Geo-environment Protection (SKLGP) in Chengdu, Sichuan province.

Type	Source	Acquisition date	Resolution (m)	Information area (%)	Usage
Images	Spot 5	Jul 2005	2.5	95	Generating landslide inventories
	Arial photographs	May 2008	1	69	
	Spot 5	July 2008	2.5	74	
		Feb 2009	2.5	100	
	Worldview 2	Apr 2011	1	100	
	Pleiades	Apr 2013	0.5	69	
	Spot 6	Apr 2015	1.5	97	
DEM	Government, academic institute	Pre-earthquake	25	-	Digitizing landslides, factor analysis
Lithology	Official geology map, Geological Survey	-	-	-	Factor analysis
Peak rainfall intensity and cumulative precipitation	Tang et al. (2009)	2008	-	-	Analyzing post-seismic landslide activities
	Luo et al. (2010)	2009	-	-	
	Ma et al. (2011)	2010		-	
	Rain gauges installed by SKLGP	2011-2015		-	

Table 1 Data used in this research. The two images taken in 2008 have 7 % of the study area covered by clouds on both images. The other images are cloud free. Information area (%) represents the percentage of the area not covered by clouds and inside of the image boundaries.

Multi-temporal landslide inventories

Digital stereoscopic image interpretation was used for mapping the landslide inventories. The images were combined with the DEM, and a series of artificial stereo images were generated using ArcScene. Co-seismic landslides were digitized first. We carefully compared the pre-and post-earthquake images to determine which of the landslides were co-seismic, and which were already existing before the earthquake. Existing landslide inventories, generated by Gorum et al. (2011), Dai et al. (2011a), Xu et al. (2014), and Li et al. (2014) were evaluated. These inventories didn't match very well with each other, and also not with the geo-rectified remote sensing images used in this study. Therefore, also co-seismic landslide inventory mapping was carried out new for the study area. The mapping accuracy was kept at

Nat. Hazards Earth Syst. Sci. Discuss., doi:10.5194/nhess-2016-193, 2016
Manuscript under review for journal Nat. Hazards Earth Syst. Sci.
Published: 3 June 2016

Natural Hazards and Earth System Sciences
Discussions

a high level by comparing the landslides on different images and by checking the landslides in the field. All the landslides were categorized based on the system proposed by British Geological Survey (BGS) which follows the scheme based on Varnes (1978) and Cruden and Varnes (1996). The landslides were classified by their material component and mass movement types (Fig. 2). Two types of material were differentiated: debris and rock. Debris, a mixture of soil and rock fragments, was interpreted from images when a fine material texture covers most of the deposition area. The parent material was interpreted as rock when rock fragments or blocks or textures of rock deposits could be clearly seen on the images. Comparing images of different years also helped to distinguish debris and rock, since landslides with rock blocks are re-vegetated much slower than debris related mass movements, even when there is no further landslide activity observed.

We differentiated the following mass movement types: fall, slide and flow. In the case of fall, materials fall from steep cliffs, with little additional displacement. Bedrock can be seen very clearly in the scarp area and the accumulation area often tends to be cone-shaped. Slide-type movements are characterized by clear back scarps, and the identification of a sliding mass, either translational or rotational in form. Flow-type movements are mostly confined to channels and occur mostly as debris flows.

Also combinations of movement types have been observed. The most frequent combinations were combinations of slide and flow, and slide and fall. Fall-slide, a combination of fall and sliding, can be observed when a fall-type movement occurs on a steep slope and the deposits slide down further during or after deposition. Slide-fall movements initiate as a slide on top of a steep cliff, and the slided materials subsequently fall over the cliff. A very common combination of landslide types is slide-flow, where the source areas of a debris flow are formed by one or more slide-type movements. This is more difficult to identify in the post-seismic landslides since they are often caused by a combination of initiation features, such as accelerated erosion, bank failure and shallow landslides in the sediment source areas. For post-earthquake landslide inventories we only use the types fall, slide and flow to represent their movement types, since the combined types are difficult to identify for reactivations of co-seismic landslides and the predominance of debris flows caused by different processes made it problematic to differentiate.

The earthquake induced landslides were interpreted using an ortho-rectified mosaic of very high resolution colour aerial photographs taken shortly after the earthquake and two Spot 5 images: one from 2005 and the other one taken shortly after the earthquake. The satellite image from 2005 revealed almost no landslide activity prior to the earthquake. Landslides were identified based on image characteristics such as tone, texture, shape and pattern, and using topographic, vegetation and drainage indicators identified through stereoscopic image interpretation (Soeters and Van Westen, 1996). Individual landslides were identified based on their unique scarp areas, even though the accumulation areas were often merged downslope. Each landslide polygon was assigned a unique identifier. Areas covered by clouds were digitized, and were not considered for the 2008 – 2009 change analysis.

Nat. Hazards Earth Syst. Sci. Discuss., doi:10.5194/nhess-2016-193, 2016
Manuscript under review for journal Nat. Hazards Earth Syst. Sci.
Published: 3 June 2016

Natural Hazards and Earth System Sciences
Discussions
Open Access
EGU

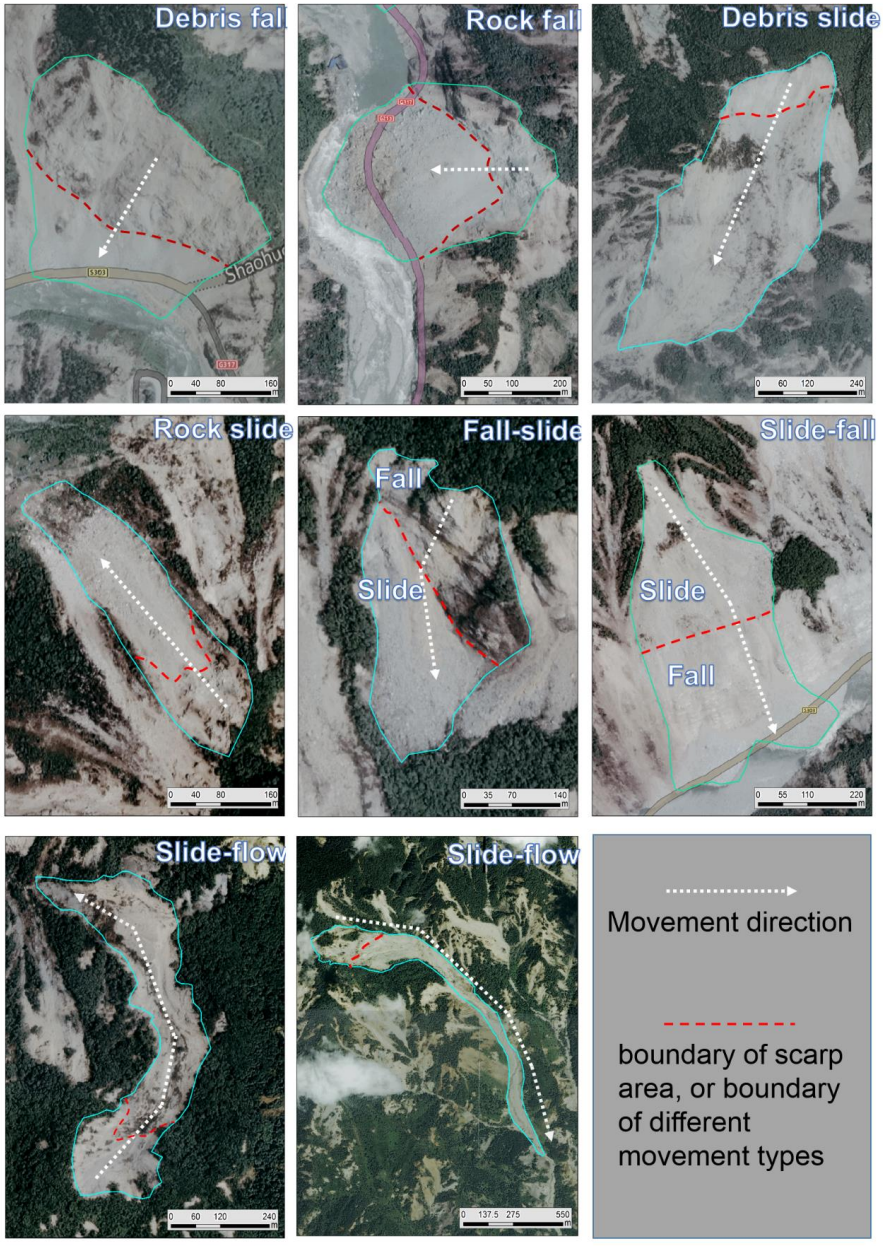

Figure 2 Examples of landslide classifications used.

The interpretation of post-earthquake landslides was carried out by comparing remote sensing images of different years, starting from the earliest post-earthquake image in 2009. The co-seismic landslide inventory was used as the basis for the inventory of the post-earthquake landslides of the following year. Then this inventory was used as the basis for the next, and so on. All landslide polygons from the co-

Nat. Hazards Earth Syst. Sci. Discuss., doi:10.5194/nhess-2016-193, 2016
Manuscript under review for journal Nat. Hazards Earth Syst. Sci.
Published: 3 June 2016

Natural Hazards and Earth System Sciences
Discussions

seismic landslide inventory were classified for each period with a *landslide activity level* and a *vegetation cover* level. Changes caused by the enlargement of existing landslides and newly triggered landslides were included in the digital inventories, and also changes in landslide classifications were marked in the associated attribute tables. If in a later year landslide activity was confined within the polygon of a pre-existing landslide, no digitization was done and the polygon of the pre-existing landslide was assigned with a landslide activity class value based on the level of the activity. This was done for all the consecutive years. If there is no activity in a pre-existing landslide polygon, the landslide is considered as a dormant landslide. Several tools in ArcMap were used to calculate attributes for the landslide polygons related to area, slope, aspect, and major lithology in the landslide polygons. The attribute table of the landslide inventories is shown in Table 2.

The *landslide activity levels* were defined based on the changes in the diagnostic features between remote sensing images taken in different periods. The vegetation cover alone does not determine whether a landslide is active or not. A landslide can be bare and dormant, or partly covered by vegetation and active. The following landslide activity classes were used: level 0, no landslide activity and the landslide is dormant; level 1, less than 1/3 of the area of a landslide is active; level 2 about 1/3 to 2/3 of the area of a landslide is active; level 3, more than 2/3 of a landslide is active or the landslide is newly formed.

The *vegetation cover level* was judged by the area of vegetation cover on landslides and was classified into four classes: level 0, most area of the landslide is covered by vegetation; level 1, more than 2/3 of the landslide is covered by vegetation; level 2, 1/3 to 2/3 of the landslide is covered by vegetation; level 3, less than 1/3 of the area of a landslide is covered by vegetation;

Attributes	Description
ID	Landslide identifier
Material	The material component of the landslide (rock or debris)
Mass movement type	The mass movement type (fall, slide, flow, fall-slide or slide-flow)
No information	The landslide is covered by clouds or located outside of the image boundary
Landslide activity level	The landslide activity class (0: dormant; 1: < 1/3 active, 2: 1/3 – 2/3 active; 3: > 2/3 active).
Vegetation cover level	The vegetation cover class (0: vegetated; 1: > 2/3 vegetated, 2: 1/3 – 2/3 vegetated; 3: < 1/3 vegetated).
New landslide	Landslide that does not occur on pre-existing landslide. The year in which it is first seen is indicated
Area	The area of the landslide in m^2
Lithology	The major lithology within the scarp area of a landslide polygon
Aspect	The orientation of slopes in the scarp area
Max slope angle	The highest slope angle which is calculated from the DEM in a landslide polygon

Table 2 Attributes collected for the landslide inventories

Nat. Hazards Earth Syst. Sci. Discuss., doi:10.5194/nhess-2016-193, 2016
Manuscript under review for journal Nat. Hazards Earth Syst. Sci.
Published: 3 June 2016

Natural Hazards and Earth System Sciences
Discussions

Results

Co-seismic landslides

The co-seismic landslide inventory map for the study area is shown in Fig 3. The co-seismic landslide inventory contains 6727 landslides with a total area of 54.6 km^2, covering about 29.4% of the 179 km^2 interpretation area. The average and median area of the co-seismic landslides are 8122 m^2 and 2141 m^2 respectively. About 25% of all the landslides have an area of 100-800 m^2. When we apply the empirical area-volume relationships presented by Guzzetti et al. (2009), the total volume of the interpreted co-seismic landslides is 0.48 Km^3. Obviously the size of the individually mapped landslides has a large influence on the volume estimation, and the degree of generalization of a landslide inventory is therefore of importance. When we use the same relation using the inventory of Dai et al. (2011) which has large landslide polygons merging multiple individual landslides, the result is 0.63 Km^3. Most of the large earthquake-triggered landslides are in the western part of the study area, which has a steeper terrain and is closer to the epicentre. The mean size of the landslides in the western part is about 10,000 m^2. Most of the co-seismic landslides in the eastern part of the study area are small and medium-size with an average area of 3782 m^2. Table 3 shows the relation between lithology and landslides, which shows that most landslides occurred in granite and diorite.

Lithology type	Number of landslides	Number density (landslides/km^2)	Area of landslides (km^2)	Area density (%)
Diorite	1208	34.2	16.4	46
Granite	4713	46.4	34.1	34
Sandstone	522	48.3	2.5	23
Feldspar sandstone with shale	284	12.3	1.6	7

Table 3 The relation between lithology and co-seismic landslides

Table 4 gives a summary of the co-seismic landslide inventory mapped in this study. Debris slides were by far the most common phenomena (5604 out of a total of 6727 events) as the strong topographic amplification resulting in the failure of the weathering soil mantle on many of the steep slopes in the area. In specific locations, where the structural geology was favourable, rock slides took place along discontinuities (262 events). In a number of cases the presence of steep cliffs resulted in fall type of movements (513 events) or a combination of fall and slide types (177). It is remarkable that the number of flow-related co-seismic mass movements was relatively limited (171 cases) which is also due to the fact that the earthquake occurred during the dry season.

	Slide	Fall	Fall-slide	Slide-flow	Sum
Debris	5604	272	124	171	6171
Rock	262	241	53	0	556
sum	5866	513	177	171	6727

Table 4 co-seismic landslide types

Nat. Hazards Earth Syst. Sci. Discuss., doi:10.5194/nhess-2016-193, 2016
Manuscript under review for journal Nat. Hazards Earth Syst. Sci.
Published: 3 June 2016

Natural Hazards and Earth System Sciences
Discussions

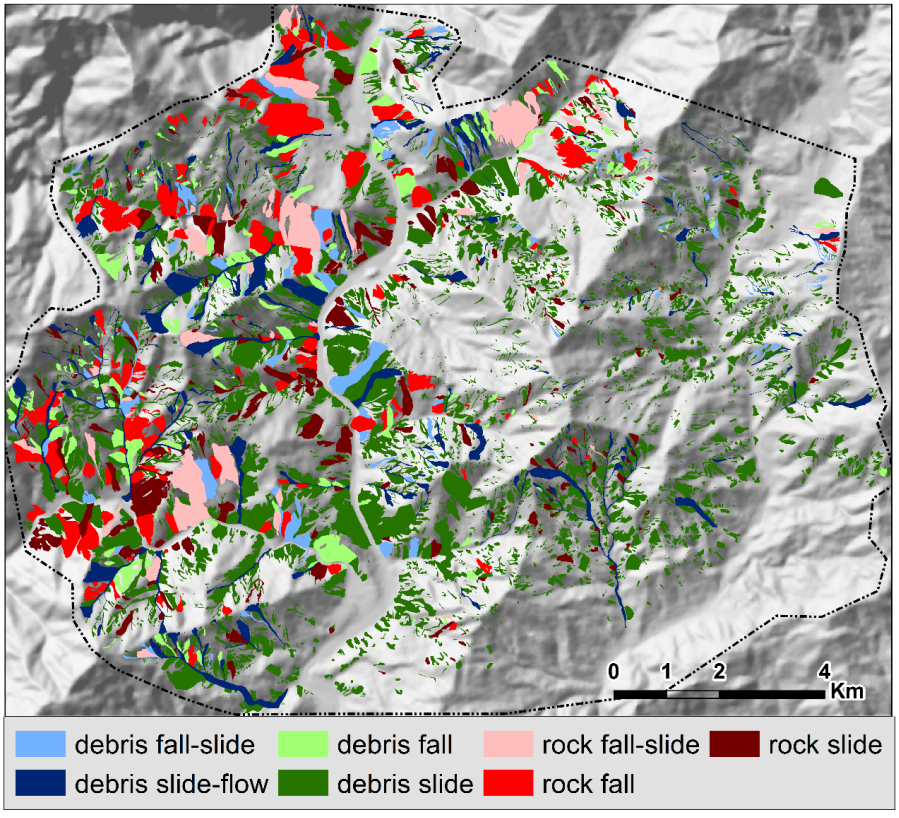

Figure 3 Co-seismic landslide inventory.

Both the number of landslides in our inventory and the area affected are much higher than the values reported by Dai et al. (2011b). They mapped only 661 landslides as polygons with a total area of 33.8 Km^2 within the Yingxiu part of the study area. Due to clouds in their available image they didn't map the landslides in the Longchi area. In our inventory, we distinguished 4175 landslides with an area of 45.9 Km^2 in the Yingxiu area. Gorum et al. (2011) mapped 1141 landslide initiation points in our interpretation area. Our inventory contained approximately 6 times more landslides than the ones detected by Dai et al. (2011) and 3.5 times more than mapped by Gorum et al (2011). The availability of very high resolution aerial photographs taken shortly after the earthquake provided better resolution and lower cloud cover than the satellite images used by the other two studies. The other two studies ignored many small landslides because they mapped the entire earthquake affected area, while we devoted our time on landslide mapping for this smaller area. Dai et al (2011) also merged several individual landslides into larger polygons (Fig.4).

Nat. Hazards Earth Syst. Sci. Discuss., doi:10.5194/nhess-2016-193, 2016
Manuscript under review for journal Nat. Hazards Earth Syst. Sci.
Published: 3 June 2016

Natural Hazards and Earth System Sciences
Discussions

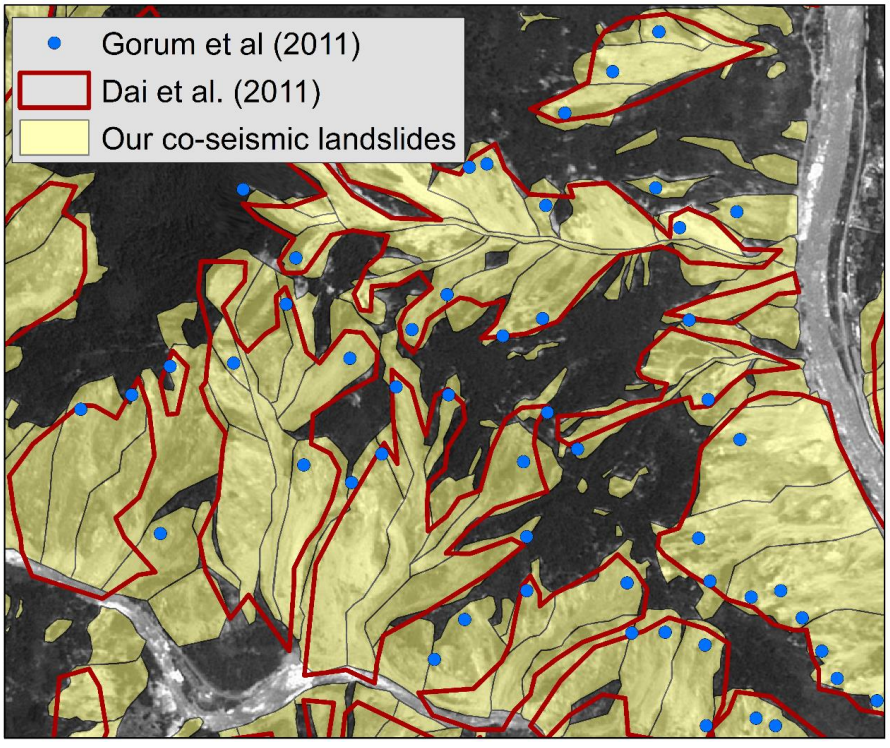

Figure 4 Comparing our inventory with the landslide initiation point inventory by Gorum et al. (2011) and the polygon-based inventory by Dai et al. (2011b) for a small part of the area

For a more detailed comparison between the observed landslide sizes of the different Wenchuan inventories, we have utilized the polygon-based Wenchuan inventories provided by Xu et al. (2014), Li et al. (2014) and Dai et al. (2011a). Since these inventories cover a much larger landslide- affected area, we have extracted the landslides located inside our study area. The inventory from Gorum et al. (2011) could not be used as it only contained points, and no polygons.

We have analysed the frequency-area distribution (FAD) of landslide areas and observed the power-law scaling (e.g. Guzzetti et al., 2002; Hovius et al., 1997; 2000; Malamud et al., 2004; Stark and Hovius, 2001) in all inventories (Fig. 5). In other words, we have observed an increasing trend in the number of the landslides from large to medium by following a power-law. For each inventory, the slope of the FAD, which is called as the power-law exponent (β), was calculated based on the method suggested by Clauset et al. (2009). The obtained β values change from 2.4 to 2.7 (Table 5), which is consistent with the literature that points out an interval having a central tendency around 2.3–2.5 (Stark and Guzzetti, 2009; Van Den Eeckhaut et al., 2007). Towards the tail of the power-law where we have fewer large landslides, the FADs of the inventories follow a similar line. Since the position of the power-law tail is assumed as the manifestation of landslide magnitude (Malamud et al., 2004), although we are analysing different inventories with a varying completeness level, we can estimate a similar magnitude for them. This observation supports the landslide event quantification theory of Malamud et al. (2004).

Nat. Hazards Earth Syst. Sci. Discuss., doi:10.5194/nhess-2016-193, 2016
Manuscript under review for journal Nat. Hazards Earth Syst. Sci.
Published: 3 June 2016

Natural Hazards and Earth System Sciences
Discussions

In all inventories, we have also observed a divergence from the power-law distribution for the small landslides. The frequency of landslide areas begins to decrease after a certain size and follows a positive power-law decay; a phenome referred to as rollover (Stark and Hovius, 2001). Since the frequency of landslide areas keeps increasing up to the rollover point, the rollover point is considered as the most frequently occurring landslide area in the inventory (e.g. Parker et al., 2015). In this regard, we have evaluated the relative completeness level of the inventories. Since the inventory of Dai et al. (2011) is one of the pioneer inventories generated soon after the Wenchuan event, it has a relatively lower resolution. The average landslide area of this inventory is around 53000m^2, while for the other inventories this value changes between 5500 m^2 and 8000 m^2 (Table 5). Therefore, in the inventory from Dai et al. (2011) the rollover point is observed around 3850 m^2, which is the largest rollover point among all the Wenchuan inventories. On the other hand, our inventory gives the lowest rollover point and it is nearly-complete up to around 340 m^2. This finding can be interpreted as the relatively higher completeness level of our inventory. The inventory of Xu et al. (2014) shows a similar completeness level as our product and it is nearly complete up to 500 m^2. Furthermore, our inventory gives relatively smoother positive power-law decay than the inventory of Xu et al. (2014). It indicates that our inventory includes a higher number of smaller landslides as compared to the inventory from Xu et al. (2014). The rollover point for the inventory of Li et al. (2014) is around 1140 m^2, and it can be considered as less complete compared to our inventory and the one by Xu et al. (2014).

Inventory	Total number of landslides	Total landslide area (km^2)	Minimum landslide area (m^2)	Maximum landslide area (m^2)	Average landslide area (m^2)	β	The approximate rollover point (m^2)
This Study	6727	54,6	30	556381	8122	2,72	340
Xu et al., 2014	7985	44,6	69	397408	5588	2,47	500
Li et al., 2014	3896	34,2	306	525126	8789	2,51	1140
Dai et al., 2011	576	30,9	714	2142126	53713	2,25	3850

Table 5 Summary information for the co-seismic landslide inventories collected for the study area. B is the power-law exponent of the frequency-area distribution (FAD).

Nat. Hazards Earth Syst. Sci. Discuss., doi:10.5194/nhess-2016-193, 2016
Manuscript under review for journal Nat. Hazards Earth Syst. Sci.
Published: 3 June 2016

Natural Hazards and Earth System Sciences
Discussions

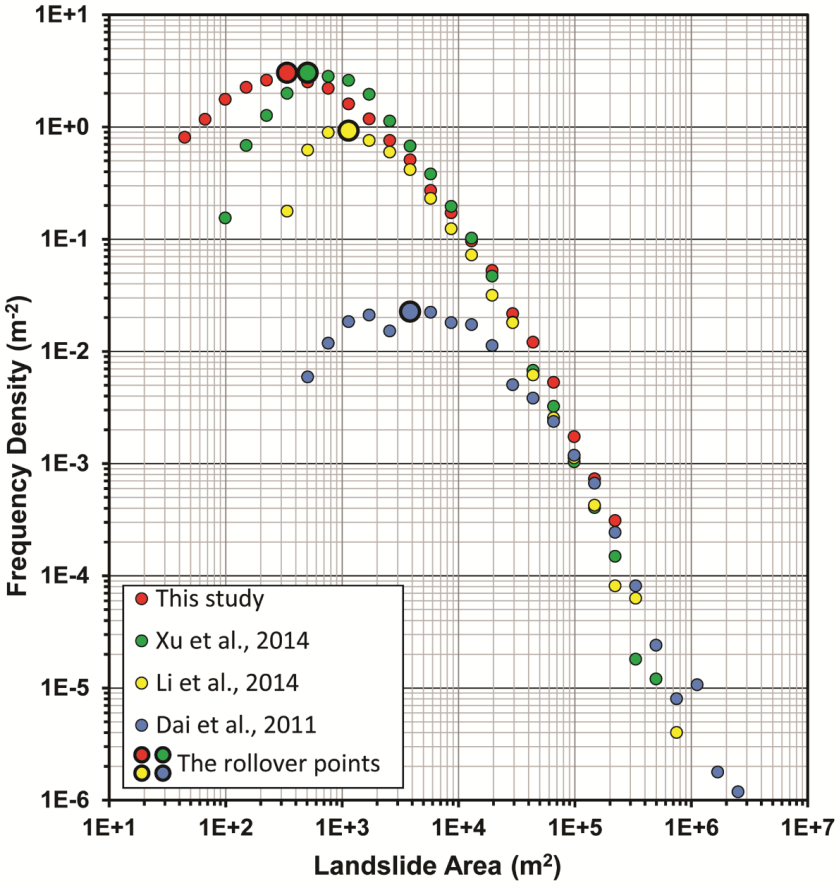

Figure 5 The frequency-area distributions (FAD) of the different co-seismic landslide inventories collected for the study area.

Post-seismic landslide inventories

In the years after the earthquake, large numbers of mass movements were induced by rain storms, whereas many others were slowly covered by vegetation regrowth. Using the available satellite images (Table 1), four new landslide inventories were generated.

An inventory for 2009 was made using a Spot 5 image from February 2009, with a spatial resolution of 2.5 meters. The inventory reflects the situation after the rainy season of 2008, during which a large number of debris flows were formed. The landslide inventory map is shown in Fig. 6. Due to cloud cover in the 2008 images, part of the landslide changes in the eastern side could not be identified. Even though there had been significant rainfall events in the monsoon of 2008, the number of active landslides was reduced to 967 including an additional 83 new landslides. Most of the active landslides (69%) were debris flows. Except for the areas covered by clouds in the 2008 images, 13% of the earthquake triggered

Nat. Hazards Earth Syst. Sci. Discuss., doi:10.5194/nhess-2016-193, 2016
Manuscript under review for journal Nat. Hazards Earth Syst. Sci.
Published: 3 June 2016

276 landslides were reactivated.

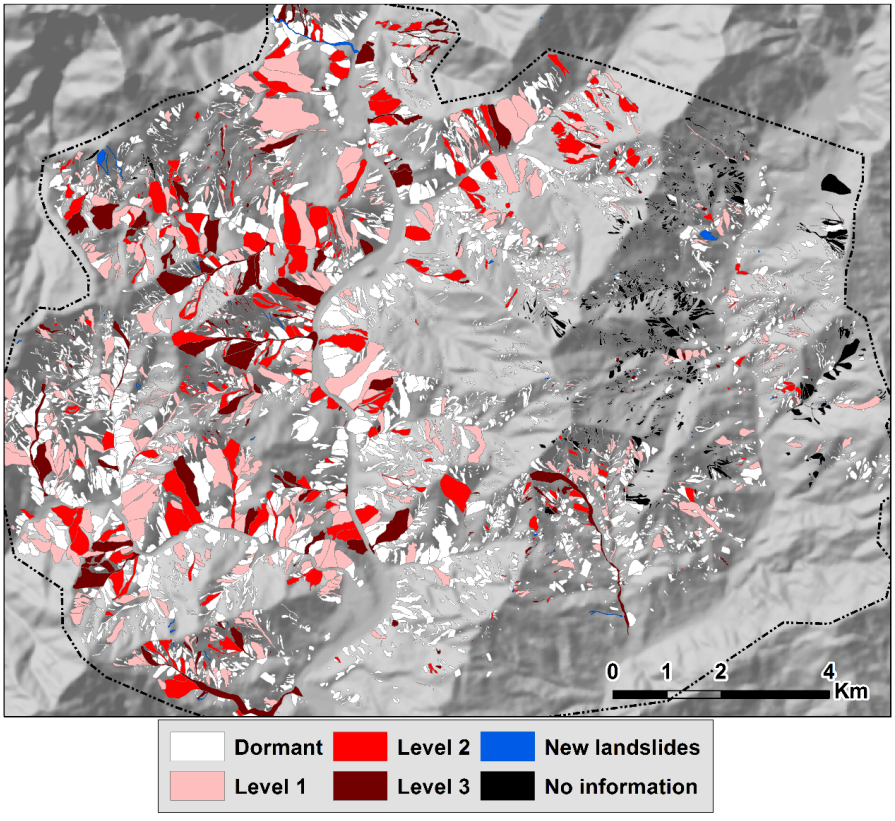

277

278 **Figure 6 Landslide inventory mapped based on the image taken in February 2009, reflecting the**
279 **situation after the rainy season of 2008.**

280

281 We were not able to find suitable images for 2010, therefore we decided to make a new inventory every
282 two years after the earthquake. The next landslide inventory was made based on a Worldview Image
283 from April 2011 with 1-meter spatial resolution. The image was cloud free except for a small area in the
284 eastern side. In this inventory 28% of the pre-existing landslides were active during this period, and the
285 number of active landslides has increased significantly to 2633, 66% of which are debris flows. As can
286 be seen from Figure 7 this inventory is almost complete for the entire area. There were also 569 new
287 landslides mapped between 2009 and 2011. This indicates that between February 2009 and April 2011
288 there have been one of more extreme rainfall events, which will be further discussed in the next section.

Nat. Hazards Earth Syst. Sci. Discuss., doi:10.5194/nhess-2016-193, 2016
Manuscript under review for journal Nat. Hazards Earth Syst. Sci.
Published: 3 June 2016

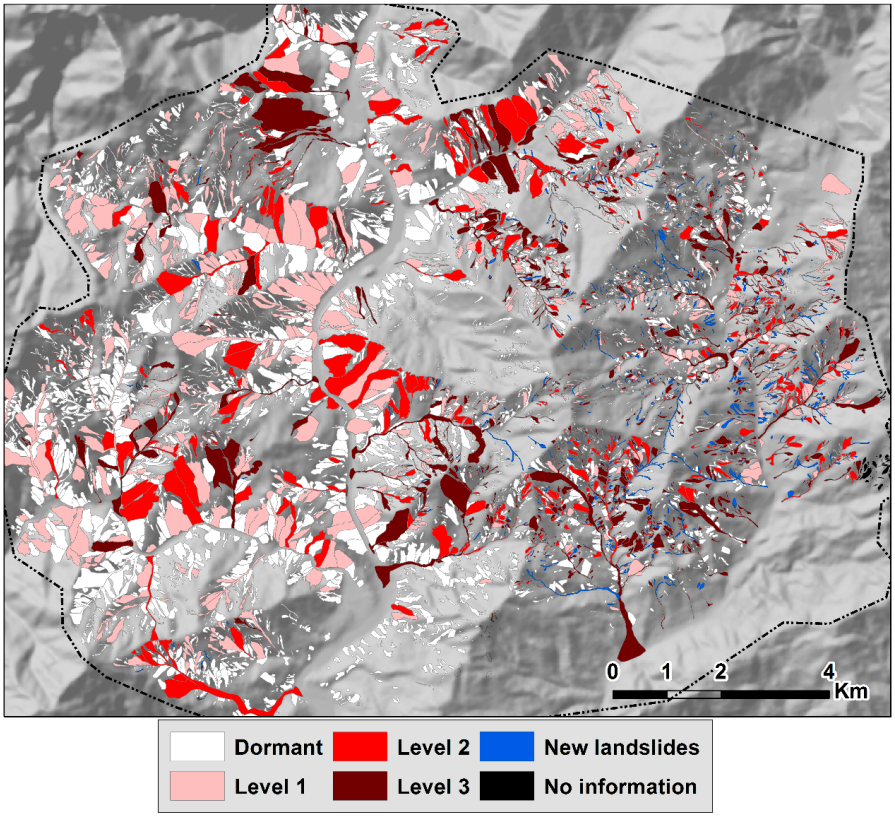

289
290 **Figure 7 Landslide inventory mapped based on the image taken in April 2011, reflecting the**
291 **situation after the rainy seasons of 2009 and 2010.**
292
293 A Pleiades image from April 2013, with a spatial resolution of 0.5 meters, was used to map the next
294 landslide inventory. However, due to the different image size, only 69% of the interpretation area could
295 be mapped in 2013 (Fig. 8). It is obvious that the activity levels in 2013 were much lower than in the
296 previous periods. Except for the areas outside the image boundary, only 3% of the pre-existing landslides
297 were active and 88% of them were identified with a landslide activity level 1 (dormant).

Nat. Hazards Earth Syst. Sci. Discuss., doi:10.5194/nhess-2016-193, 2016
Manuscript under review for journal Nat. Hazards Earth Syst. Sci.
Published: 3 June 2016

Natural Hazards and Earth System Sciences
Discussions
Open Access
EGU

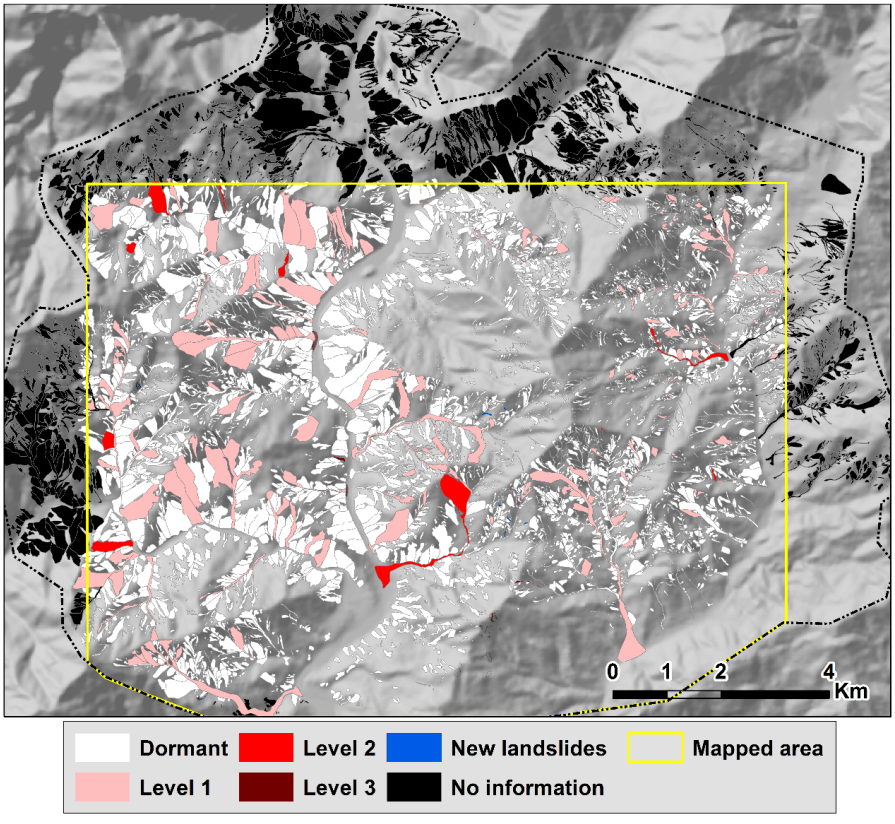

298

299 **Figure 8 Landslide inventory mapped based on the image taken in Apr 2013, reflecting the**
300 **situation after the rainy season of 2011 and 2012. The actual mapped area was limited within the**
301 **yellow polygon due to the smaller area covered by the available Pleiades image.**

302

303 The last landslide inventory map was made using a Spot 6 image, with a spatial resolution of 1.5 meter
304 from April 2015. This image covers most of the study area except for a small part in the North (Fig. 9).
305 Only 66 active landslide are identified on the image, of which only two were new landslides. Less than
306 1% of the pre-existing landslides were active. Compared with the images of the earlier period, the
307 vegetation cover on landslides in 2015 was significantly higher.

Nat. Hazards Earth Syst. Sci. Discuss., doi:10.5194/nhess-2016-193, 2016
Manuscript under review for journal Nat. Hazards Earth Syst. Sci.
Published: 3 June 2016

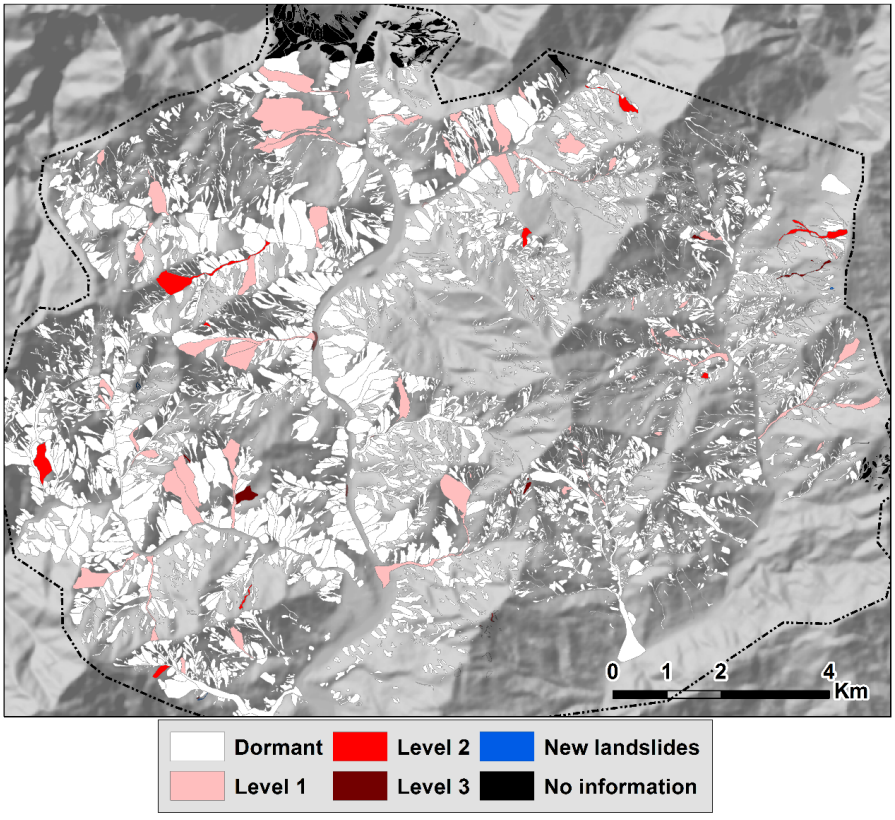

Figure 9 Landslide inventory mapped based on the image taken in Apr 2015, reflecting the situation after the rainy seasons of 2013 and 2014.

After the earthquake, from 2008 till April 2015, the number of landslides (including the dormant landslides) in the study area increased by 660, to a total of 7387. The total landslide area increased from 54.6 km^2 to 58.3 km^2. This indicates that the landslide activity in the post-earthquake period was not restricted to the co-seismic landslide area only. This is important to consider when making post-earthquake reconstruction planning in other mountainous environments. Landslide activity evolved in different ways. The first type of reactivation observed was by slide-type movements of the bare surfaces of co-seismic landslides. Also flow-type movement caused by run-off erosion in the landslide deposits of the pre-existing landslides, with deposition either occurring on top of earlier debris flow materials, or covering new areas. This was considered as the main cause for the enlargement of co-seismic landslides. The third observed mechanism was a retrogressive activity of the scarps in the initiation area. Of the total of 6727 co-seismic landslides, 2221 had one or more phases of reactivation after they were triggered by the earthquake until April 2015. The most frequent post-earthquake landslide type is flow, accounting for 66% of all the active landslides in the post-earthquake inventories. Table 6 summarizes the statistics of the four post-earthquake landslide inventories.

Nat. Hazards Earth Syst. Sci. Discuss., doi:10.5194/nhess-2016-193, 2016
Manuscript under review for journal Nat. Hazards Earth Syst. Sci.
Published: 3 June 2016

Natural Hazards and Earth System Sciences Discussions

Activity level	Fall	Slide	Flow	Sum by activity level
The inventory of 2009				
No information				988
0				4855
1	8	91	353	452
2	2	73	175	250
3	0	70	112	182
New landslide	1	51	31	83
Sum by movement type	11	285	671	6810(1) 967(2)
The inventory of 2011				
No information				44
0				4718
1	7	182	622	811
2	2	180	323	505
3	4	292	436	732
New landslide	1	215	353	569
Sum by movement type	14	869	1734	7379(1) 2617(2)
The inventory of 2013				
No information				1862
0				5348
1	2	3	149	154
2	0	0	12	12
3	0	0	3	3
New landslide	0	4	2	6
Sum by movement type	2	7	166	7385(1) 175(2)
The inventory of 2015				
No information				150
0				7171
1	0	3	41	44
2	0	1	9	10
3	0	3	7	10
New landslide	0	0	2	2
Sum by movement type	0	7	59	7387(1) 66(2)

328 **Table 6 Statistics of the post-earthquake landslide inventories. (1) The total number of landslides**
329 **in each inventory including those without information (which are either located in cloud covered**

Nat. Hazards Earth Syst. Sci. Discuss., doi:10.5194/nhess-2016-193, 2016
Manuscript under review for journal Nat. Hazards Earth Syst. Sci.
Published: 3 June 2016

Natural Hazards and Earth System Sciences
Discussions

areas, or areas outside of the image boundaries). (2) The total number of landslides in each inventory excluding those without information, and those that are dormant (activity level 0).

In general the landslide activity decreased considerably from May 2008 until April 2015, with a total of active landslides reducing from 6727 co-seismic landslides to 66 active landslides in 2015. After the 2010 monsoon season, the activity of the post-earthquake landslides dropped considerably and most of the active landslides were marked with activity level 1 (Fig. 11). Table 6 shows details of the landslide activity changes for the various inventories. Between the inventories of 2009 and 2011, at least 1834 landslides had an increased activity level. About half of the active landslides in the 2011 inventory are co-seismic which were dormant in the 2009 inventory, and 39% of the active landslides in the inventory of 2009 became dormant in 2011. From April 2011 to April 2013, 66% of the active landslides in the inventory of 2011 became dormant in the inventory of 2013. Sixty-five percent of the active landslides in 2013 are active pre-existing landslides with a higher activity class level in 2011. During April 2013 to April 2015, 90% of the active landslides in the inventory of 2013 became dormant, 44% of the active landslides in 2015 kept the same activity level as in 2013, and 46% of the active landslides occurred on pre-existing landslides that were dormant in 2013. We can conclude from this analysis that the pattern of active landslides changes constantly over time. It is not possible to predict after the earthquake which landslides will remain active over the next decade, as this pattern changes constantly, most probably related to the specific variation of rainfall intensity during rainstorms in the post-earthquake period.

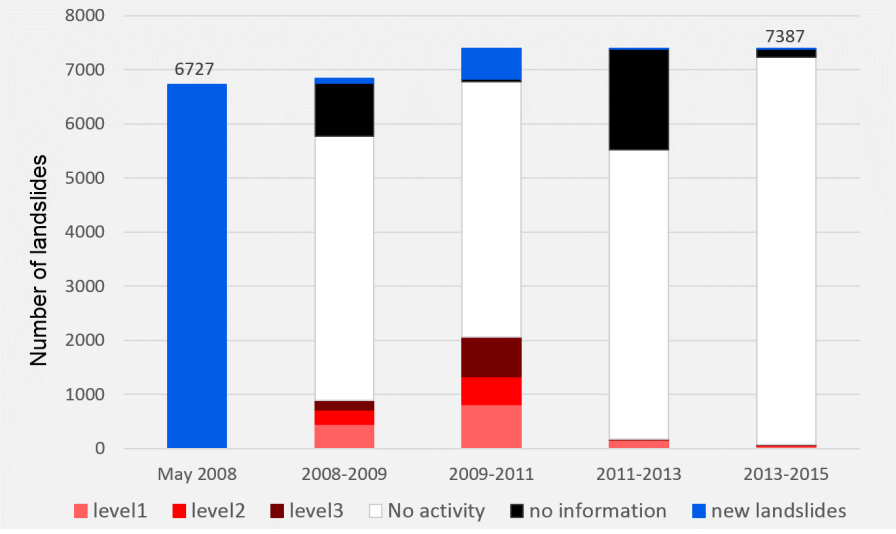

Figure 10 Activity levels of the five landslide inventories.

Most of the new landslides occurred during the period of 2009-2011. The most frequent landslide type for the new landslides was slide (60.4%), followed by flow (36%) and fall. The average area of the new landslides is 1339 m^2, with a range from 34 m^2 to 31356 m^2. The large new landslides are mainly debris flows with long run-out distances. Overall the new landslides are mainly small and medium-sized landslides: 90% of the new landslides are less than 3023 m^2.

Nat. Hazards Earth Syst. Sci. Discuss., doi:10.5194/nhess-2016-193, 2016
Manuscript under review for journal Nat. Hazards Earth Syst. Sci.
Published: 3 June 2016

Natural Hazards and Earth System Sciences Discussions

Year	Activity level	0	1	2	3	No info	sum
2011 Inventory							
2009 Inventory	0	3710[5]	368	283	457	37	1263[1]
	1	183	148	72	52	0	
	2	89	88	44	31	0	
	3	49	65	37	31	0	
	New	58	4	3	14	0	
	No info	634	145	65	139	7	
	sum	379[2]	197[3]				237[4]
2013 Inventory							
2011 Inventory	0	3578[5]	23	3	2	1095	29[1]
	1	502	34	1	0	279	
	2	293	40	1	0	173	
	3	528	53	6	1	157	
	New	444	5	0	0	117	
	No info	1	0	0	0	43	
	sum	1767[2]	104[3]				36[4]
2015 Inventory							
2013 Inventory	0	5322[5]	7	6	7	0	22[1]
	1	132	21	1	1	0	
	2	8	3	0	0	0	
	3	3	0	0	0	0	
	New	6	0	0	0	0	
	No info	1689	20	3	2	150	
	sum	149[2]	3[3]				21[4]

Table 7 Changes in landslide activity level of the consecutive years. [1] Total number of landslides with increased activity level compared with the previous period. [2] Number of landslides that became dormant. [3] Number of landslides with decreased activity level, excluding dormant. [4] Number of landslides with the same activity level as the previous period. [5] Number of landslides that remain dormant in both inventories. The number mismatches were caused by small landslides which were ignored by ArcMap software during rasterizing the inventories to do this analysis.

When we compare the number of 66 active landslides in the inventory of 2015 with the 132 landslides recorded from 1961 to 2005 (Yang et al., 2005) in the whole 3936 km^2 Wenchuan county, the frequency of the landslide occurrence has increased significantly after the earthquake, and it is still not back to the pre-earthquake levels. It can be observed further that the increase of post-earthquake landslides both in number and in area were 8.9% and 6.8% respectively, which are much lower than observed in Taiwan after the Chi-Chi earthquake (42.8% increase in area within 2 years according to Lin et al. (2006)). The landslide increment after the Chi-Chi earthquake could be caused by its location in relation to the path of typhoons, as the areas was affected several times with rainfall events with more than 100 mm/h precipitation intensity. In the Wenchuan area, the recorded rainfall intensity and cumulative rainfall are much lower (Table 8). Also, the lithology in both areas is completely different, with the Wenchuan areas underlain mostly by volcanic rocks, while in the area affected by the Chi-Chi earthquake sedimentary

Nat. Hazards Earth Syst. Sci. Discuss., doi:10.5194/nhess-2016-193, 2016
Manuscript under review for journal Nat. Hazards Earth Syst. Sci.
Published: 3 June 2016

Natural Hazards and Earth System Sciences
Discussions

rocks and metamorphic rocks are most common (Lin et al. (2006).

Controlling factors

The large differences in landslide activity that were observed between the post-earthquake landslide inventories, especially the increase in activity observed in the 2011 inventory, were expected to be caused by differences in rainfall extreme events.

Previous works (Lin et al., 2006; Zhou et al., 2013) have indicated that the magnitude and scale of the post-seismic landslide activity is related to the spatial distribution and intensity of rainfall events. Unfortunately, there are very few rain gauges in the direct surroundings of the study area that were operational from 2008 onwards. After a large number of landslides were triggered by the storm in 2010, several rain gauges were installed in 5 catchments that were considered as highly dangerous. From the 18 available rain gauges and literature study we analysed the maximum intensity, duration and accumulated precipitation of the largest rainfall event of each year as indicators for the importance of the monsoon of that year in landslide reactivation. The rainfall data of the largest rainfall events from 2011 to 2015 are average values calculated from several rain gauges distributed across the area (Table 8).

Related inventory	Date (D/M/Y)	Peak intensity (mm/h)	Accumulated rainfall (mm)	Duration (hours)
2009	23.9.2008	60	347	10
2011	17.7.2009	70	219	6
	13.8.2010	75	229	17
2013	29.7.2011	54	150	20
	18.8.2012	39.5	117	6
2015	10.7.2013	64	108.5	6
	10.4.2014	53	53	1

Table 8 Maximum rainfall intensity, duration and accumulated rainfall of the largest rainfall events of each year. The source of rainfall data is indicated in Table 1.

The two largest rainfall events occurred during the monsoons of 2009 and 2010. They have reactivated a considerable number of landslides as can be observed from the inventory of 2011. The maximum rainfall intensity and accumulated precipitation of the monsoon of 2008 were similar with those during 2011 to 2014. However, in the 2009 inventory there were more active landslides than in the inventories of 2013 and 2015. This is due to the fact that most of the landslide scarps were not re-vegetated yet in the months following the earthquake. In 2011 many more landslides were re-vegetated and the same magnitude of rainfall reactivated much less landslides than in 2008. Also the availability of loose materials in the initiation zone was likely much less in 2011 as compared to 2008 due to landslide activity in the period in-between. The loose materials were transported downstream as debris flows (Fig. 11). The vegetation cover class on the earthquake-triggered landslides in 2008 was 3 (> 2/3 bare). In the inventory of 2009, this had changed to 2, and then 3 again in the inventory of 2011 due to massive landslide reactivations. The value was lowered to 1 (<1/3 bare) in the inventory of 2015.

Nat. Hazards Earth Syst. Sci. Discuss., doi:10.5194/nhess-2016-193, 2016
Manuscript under review for journal Nat. Hazards Earth Syst. Sci.
Published: 3 June 2016

Natural Hazards and Earth System Sciences
Discussions

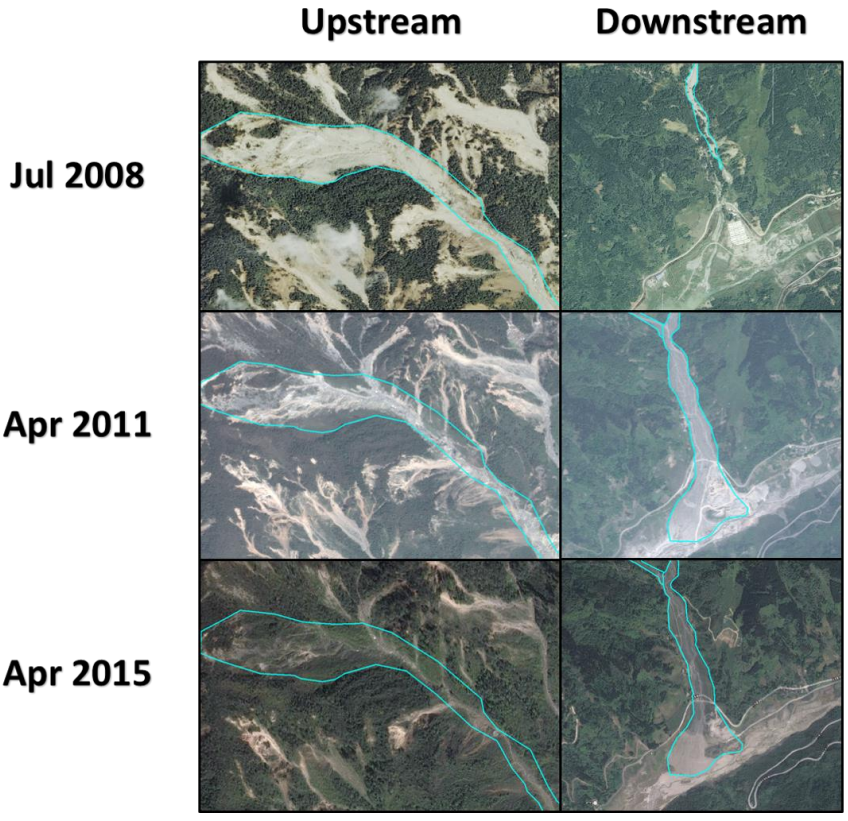

Figure 11 Examples of changes in landslide activity in the source and deposition areas of a typical debris flow gulley. In 2008 the loose materials produced by this co-seismic landslide were still located in the valley in the upslope part. After three rainy seasons, debris flows and erosion transported the materials to the downstream area. In 2015, most of the upstream area was covered by vegetation again, and debris flow activity in the downstream part had reduced considerably.

The pattern of reactivation of landslides can also be related to different spatial distributions of the rainfall events that occurred in the period in between two dates for which landslide inventories are available. However, the available rainfall data didn't allow us to generate rainfall distribution maps for the various landslide events. This should be investigated further in future.

The relation between landslide activity changes and topographic factors, such as slope direction, and slope angle were also analysed, and also the relation with lithology. We calculated the ratio of the area of active landslides over the total landslide area within each factor class. The results indicate that aspect is not a significant factor in determining the presence of active post-seismic landslides. In the areas with granite, diorite and sandstone the percentage of active landslides were 41%, 28% and 43% respectively. The areas with other lithology types were too small in size to make a proper analysis. A comparison of active landslide percentages for different slope classes showed that slopes steeper than 20 degrees had a much higher degree of reactivation. However, lower slope angles occurring in the channels and alluvial

Nat. Hazards Earth Syst. Sci. Discuss., doi:10.5194/nhess-2016-193, 2016
Manuscript under review for journal Nat. Hazards Earth Syst. Sci.
Published: 3 June 2016

fans also had a very high percentage of landslide activity, caused by the occurrence of debris flow deposits.

There is also an important difference in active landslide percentage when comparing the western (Yingxiu) and the eastern part (Longchi). The Yingxiu area had much more and larger sized co-seismic landslides than the Longchi area. However in the 2011 inventory, the eastern part had 46% of the landslides active which is 22% more than the western part. This was caused by the large amount of new landslides in the eastern part, which contained 83% of all new landslides. This phenomenon indicates that the effect of the earthquake was much stronger in the western part, which had more rugged topography, where the weathering soil mantle was removed by co-seismic landslides. This was different in the eastern area, where there were less co-seismic and more post-seismic landslides. Some slopes were loosened by the earthquake but did not yet fail immediately after the earthquake, and in later years landslides were triggered by large rainfall on those unstable slopes.

Discussion and conclusions

We analysed changes in landslide activity in a period of seven years after the 2008 Wenchuan earthquake, with five multi-temporal landslide inventories, which we interpreted stereoscopically from high resolution images, followed by field investigation. The results show that most of the post-seismic landslide activities were concentrated within the first three years following the earthquake. The landslide activity decreased considerably from May 2008 until April 2015, from 6727 co-seismic landslides to 66 active landslides in 2015. After the 2010 monsoon season, the activity of the post-earthquake landslides dropped considerably and most of the active landslides became dormant. Of the total of 6727 co-seismic landslides, 2221 had one or more phases of reactivation. Apart from the reactivation of co-seismic landslides also 660 new landslides occurred after 2008. This indicates that the landslide activity in the post-earthquake period was not restricted to the co-seismic landslide area only. This is important to consider when making post-earthquake reconstruction planning in other mountainous environments.

In the digital stereo image interpretation we did not adopt a minimum threshold for landslide area. When comparing our results with other landslide inventories in this area through frequency-area distribution (FAD) our inventory shows the highest level of completeness, the highest number of small landslides, and also the highest total landslide area. However, the inventory also shows a lower total landslide volume calculated from the empirical method presented by Guzzetti et al. (2009). This might be an indication that the number and area of the landslides reported so far for the whole earthquake-hit area may be under estimated and the volume could be overestimated.

In this study we were able to devote more time on this local scale area to make a detailed landslide mapping than the previous studies which were mapping the entire earthquake- affected area. We were also able to collect more high resolution remote sensing image data than previous studies. Also the use of digital stereo image interpretation was important for mapping landslide boundaries and making landslide classifications. However, the mapping process was much more time consuming, as compared to semi-automatic image classification or monoscopic image interpretation procedures. The mapping process also requires specific skills and different people can produce different image interpretation results. We included an extensive procedure for double checking the mapped landslides by different

Nat. Hazards Earth Syst. Sci. Discuss., doi:10.5194/nhess-2016-193, 2016
Manuscript under review for journal Nat. Hazards Earth Syst. Sci.
Published: 3 June 2016

interpreters in order to ensure consistency of the inventory. The largest differences in interpretation occurred in areas with very steep and complex slopes, where the terrain could not be represented well due to the relatively poor quality of the available DEM. When determining the activities of the post-earthquake landslides, we carefully compared the images from different periods, looking for differences in the image characteristics. This gave us more detailed results compared with common landslide mapping methods which define landslides activity directly from vegetation cover, and allowed us to distinguish the actual active landslide from dormant bare landslides.

Though the landslide activity reduced after April 2011, extreme rainfall events could still trigger large amount of landslides. After the extreme rainstorm in August 2010, there have not been any other extreme rainfall events up to 2015 in the area. However, we can observe in recent images and fieldwork, that there are still large volumes of loose materials on the slopes and in the upper parts of the catchments. Though these areas mostly being covered by vegetation re-growth, they could be activated by extreme rainfall events. In the coming years and decade the chance of landslide re-activation will be determined by the speed of vegetation re-growth, the available volumes of loose materials and the occurrence of extreme rainfall events. The limited available rainfall data show that the rainfall threshold to trigger landslides is rising, leading to less landslides in the last two inventories. However, we lack enough rainfall data to do a comprehensive rainfall threshold analysis. Also we were only able to estimate landslide volumes using an empirical method. The actual volume of landslides in the area is unknown due to the lack of a high-resolution pre-earthquake DEM. It is still hard to make a prediction of how long will it take before landslide activity is back at pre-earthquake levels. Monitoring landslide activities over a longer period is required.

During our mapping process we have noticed that the large co-seismic landslides (like the one in Fig. 11), are very likely to generate major debris flows in future. Eleven out of eighteen co-seismic landslides with an area larger than 20,000 m^2 had the highest level of activity recorded and six of them had the second highest level in the post-seismic landslide inventories. All the recorded large debris flows in the area were initiated from these eleven large landslides. In some of the downstream parts, extensive debris flow mitigation works have been carried out, although some of these have been destroyed or almost covered by debris. It is recommended to monitor the activity of these large landslides, and in some cases early warning systems have already been installed.

We also recommend to continue the monitoring of landslides through image analysis. Beside remote sensing images, multi-temporal DEMs generated from Lidar data and UAV photogrammetry can be useful for monitoring, and quantifying the changes. Rainfall data with good spatial and temporal resolution, essential for designing early warning system, should also be collected to make a comprehensive rainfall threshold analysis.

We can conclude from this analysis that the pattern of active landslides changes constantly over time. It is not possible to predict after the earthquake which landslides will remain active over the next decade, as this pattern changes constantly, most probably related to the specific variation of rainfall intensity during rainstorms in the post-earthquake period.

Nat. Hazards Earth Syst. Sci. Discuss., doi:10.5194/nhess-2016-193, 2016
Manuscript under review for journal Nat. Hazards Earth Syst. Sci.
Published: 3 June 2016

Acknowledgements

The authors would like to thank the State Key Laboratory for Geohazard Prevention and Environmental Protection (SKLGP), Chengdu, China, for providing data and support with the fieldwork. We would like to thank the EU FP7 Copernicus project INCREO (http://www.increo-fp7.eu/) for providing some of the satellite data. We thank MSc students Yu Yang, Yi Wang and Chenhao Xia in SKLGP for helping us to prepare the landslide inventories. We also thank Theo Van Asch for giving useful advice for this research.

References

Chang, K.-J., Taboada, A., Chan, Y.-C., and Dominguez, S., 2006, Post-seismic surface processes in the Jiufengershan landslide area, 1999 Chi-Chi earthquake epicentral zone, Taiwan: Engineering Geology, v. 86, no. 2-3, p. 102-117.

Cheng, J. D., Huang, Y. C., Wu, H. L., Yeh, J. L., and Chang, C. H., 2005, Hydrometeorological and landuse attributes of debris flows and debris floods during typhoon Toraji, July 29–30, 2001 in central Taiwan: Journal of Hydrology, v. 306, no. 1-4, p. 161-173.

Clauset, A., Shalizi, C. R., and Newman, M. E., 2009, Power-law distributions in empirical data: SIAM review, v. 51, no. 4, p. 661-703.

Cruden, D. M., and Varnes, D. J., 1996, Landslides: investigation and mitigation. Chapter 3-Landslide types and processes: Transportation research board special report, no. 247.

Dai, F., Xu, C., Yao, X., Xu, L., Tu, X., and Gong, Q., 2011a, Spatial distribution of landslides triggered by the 2008 Ms 8.0 Wenchuan earthquake, China: Journal of Asian Earth Sciences, v. 40, no. 4, p. 883-895.

Dai, F. C., Xu, C., Yao, X., Xu, L., Tu, X. B., and Gong, Q. M., 2011b, Spatial distribution of landslides triggered by the 2008 Ms 8.0 Wenchuan earthquake, China: Journal of Asian Earth Sciences, v. 40, no. 4, p. 883-895.

Dong, J.-J., Li, Y.-S., Kuo, C.-Y., Sung, R.-T., Li, M.-H., Lee, C.-T., Chen, C.-C., and Lee, W.-R., 2011, The formation and breach of a short-lived landslide dam at Hsiaolin village, Taiwan — part I: Post-event reconstruction of dam geometry: Engineering Geology, v. 123, no. 1-2, p. 40-59.

Fan, J. C., Liu, C. H., Wu, M. F., and Yu, S. K., 2003, Determination of critical rainfall thresholds for debris-flow occurrence in central Taiwan and their revision after the 1999 Chi-Chi great earthquake, Rotterdam, Millpress Science Publishers, Debris-Flow Hazards Mitigation: Mechanics, Prediction, and Assessment, Vols 1 and 2, 103-114 p.:

Gorum, T., Fan, X., van Westen, C. J., Huang, R. Q., Xu, Q., Tang, C., and Wang, G., 2011, Distribution pattern of earthquake-induced landslides triggered by the 12 May 2008 Wenchuan earthquake: Geomorphology, v. 133, no. 3-4, p. 152-167.

Guzzetti, F., Ardizzone, F., Cardinali, M., Rossi, M., and Valigi, D., 2009, Landslide volumes and landslide mobilization rates in Umbria, central Italy: Earth and Planetary Science Letters, v. 279, no. 3-4, p. 222-229.

Guzzetti, F., Malamud, B. D., Turcotte, D. L., and Reichenbach, P., 2002, Power-law correlations of landslide areas in central Italy: Earth and Planetary Science Letters, v. 195, no. 3, p. 169-183.

Harp, E. L., and Jibson, R. W., 1995, Inventory of landslides triggered by the 1994 Northridge, California earthquake: U.S. Geological Survey Open-File Report, v. 95-213.

553 Harp, E. L., Wilson, R. C., and Wieczorek, G. F., 1981, Landslides from the February 4, 1976,Guatemala
554 Earthquake: U.S. Geological Survey Professional Paper, v. 1204-A.
555 Hovius, N., Meunier, P., Lin, C.-W., Chen, H., Chen, Y.-G., Dadson, S., Horng, M.-J., and Lines, M., 2011,
556 Prolonged seismically induced erosion and the mass balance of a large earthquake: Earth and
557 Planetary Science Letters, v. 304, no. 3–4, p. 347-355.
558 Hovius, N., Stark, C. P., and Allen, P. A., 1997, Sediment flux from a mountain belt derived by landslide
559 mapping: Geology, v. 25, no. 3, p. 231-234.
560 Hovius, N., Stark, C. P., Hao-Tsu, C., and Jiun-Chuan, L., 2000, Supply and removal of sediment in a
561 landslide-dominated mountain belt: Central Range, Taiwan: The Journal of Geology, v. 108, no.
562 1, p. 73-89.
563 Huang, R., and Fan, X., 2013, The landslide story: Nature Geosci, v. 6, no. 5, p. 325-326.
564 Li, G., West, A. J., Densmore, A. L., Jin, Z., Parker, R. N., and Hilton, R. G., 2014, Seismic mountain building:
565 Landslides associated with the 2008 Wenchuan earthquake in the context of a generalized
566 model for earthquake volume balance: Geochemistry, Geophysics, Geosystems, v. 15, no. 4, p.
567 833-844.
568 Lin, C.-W., Liu, S.-H., Lee, S.-Y., and Liu, C.-C., 2006, Impacts of the Chi-Chi earthquake on subsequent
569 rainfall-induced landslides in central Taiwan: Engineering Geology, v. 86, no. 2-3, p. 87-101.
570 Lin, G.-W., Chen, H., Hovius, N., Horng, M.-J., Dadson, S., Meunier, P., and Lines, M., 2008, Effects of
571 earthquake and cyclone sequencing on landsliding and fluvial sediment transfer in a mountain
572 catchment: Earth Surface Processes and Landforms, v. 33, no. 9, p. 1354-1373.
573 Luo, M., Wei, C., Mo, J., and Liao, W., 2010, Geo-hazard survey report of Dujiangyan: Sichuan geological
574 survey bureau.
575 Ma, y., Yu, B., Wu, Y., Zhang, J., and Qi, X., 2011, Research on the Disaster of Debris Flow of Bayi
576 Gully,Longchi,Dujiangyan,Sichuan on August 13,2010: Journal of Sichuan Universitity, v. 43.
577 Malamud, B. D., Turcotte, D. L., Guzzetti, F., and Reichenbach, P., 2004, Landslide inventories and their
578 statistical properties: Earth Surface Processes and Landforms, v. 29, no. 6, p. 687-711.
579 Shieh, C.-L., Chen, Y.S., Tsai, Y.J., Wu, J.H., 2009, Variability in rainfall threshold for debris flow after the
580 Chi-Chi earthquake in central Taiwan, China: International Journal of Sediment Research, v. 24,
581 no. 2, p. 177-188.
582 Shou, K. J., Hong, C. Y., Wu, C. C., Hsu, H. Y., Fei, L. Y., Lee, J. F., and Wei, C. Y., 2011a, Spatial and
583 temporal analysis of landslides in Central Taiwan after 1999 Chi-Chi earthquake: Engineering
584 Geology, v. 123, no. 1-2, p. 122-128.
585 Shou, K. J., Wu, C. C., Fei, L. Y., Lee, J. F., and Wei, C. Y., 2011b, Dynamic environment in the Ta-Chia
586 River watershed after the 1999 Taiwan Chi-Chi earthquake: Geomorphology, v. 133, no. 3-4,
587 p. 190-198.
588 Stark, C., and Guzzetti, F., 2009, Landslide rupture and the probability distribution of mobilized debris
589 volumes: Journal of Geophysical Research: Earth Surface, v. 114, no. F2.
590 Stark, C. P., and Hovius, N., 2001, The characterization of landslide size distributions: Geophysical
591 Research Letters, v. 28, no. 6, p. 1091-1094.
592 Tang, C., Rengers, N., van Asch, T. W., Yang, Y., and Wang, G., 2011, Triggering conditions and
593 depositional characteristics of a disastrous debris flow event in Zhouqu city, Gansu Province,
594 northwestern China: Natural Hazards and Earth System Science, v. 11, no. 11, p. 2903-2912.
595 Tang, C., Zhu, J., Li, W. L., and Liang, J. T., 2009, Rainfall-triggered debris flows following the Wenchuan
596 earthquake: Bulletin of Engineering Geology and the Environment, v. 68, no. 2, p. 187-194.

Nat. Hazards Earth Syst. Sci. Discuss., doi:10.5194/nhess-2016-193, 2016
Manuscript under review for journal Nat. Hazards Earth Syst. Sci.
Published: 3 June 2016

597 Van Den Eeckhaut, M., Poesen, J., Govers, G., Verstraeten, G., and Demoulin, A., 2007, Characteristics
598 of the size distribution of recent and historical landslides in a populated hilly region: Earth and
599 Planetary Science Letters, v. 256, no. 3, p. 588-603.
600 Varnes, D. J., 1978, Slope movement types and processes: Transportation Research Board Special
601 Report, no. 176.
602 Xu, C., Xu, X., Yao, X., and Dai, F., 2014, Three (nearly) complete inventories of landslides triggered by
603 the May 12, 2008 Wenchuan Mw 7.9 earthquake of China and their spatial distribution
604 statistical analysis: Landslides, v. 11, no. 3, p. 441-461.
605 Xu, Q., Zhang, S., Li, W. L., and van Asch, T. W. J., 2012, The 13 August 2010 catastrophic debris flows
606 after the 2008 Wenchuan earthquake, China: Natural Hazards and Earth System Science, v. 12,
607 no. 1, p. 201-216.
608 Yang, X., Zhang, Y., Hu, C., Hao, H., Huang, Y., Zhou, l., Li, G., Kong, Y., Zhen, Q., Zhang, Y., Shang, X., Jia,
609 L., and Wang, Y., 2005, Geo-hazard survey of Wenchuan county, Sichuan.
610 Zhou, W., and Tang, C., 2014, Rainfall thresholds for debris flow initiation in the Wenchuan earthquake-
611 stricken area, southwestern China: Landslides, v. 11, no. 5, p. 877-887.
612 Zhou, W., Tang, C., and Zhou, C.-h., 2013, Rainfall Patterns of Post-seismic Debris Flows in the
613 Wenchuan Earthquake Area, p. 895-900.
614